8164 *Inorg. Chem.* **2009**, *48*, 8164–8172
DOI: 10.1021/ic900607s

Inorganic Chemistry
Article

Authentic-Blue Phosphorescent Iridium(III) Complexes Bearing Both Hydride and Benzyl Diphenylphosphine; Control of the Emission Efficiency by Ligand Coordination Geometry

Yuan-Chieh Chiu,[†] Chen-Huey Lin,[†] Jui-Yi Hung,[†] Yun Chi,*[,†] Yi-Ming Cheng,[‡] Kang-Wei Wang,[‡] Min-Wen Chung,[‡] Gene-Hsiang Lee,[‡] and Pi-Tai Chou*[,‡]

[†]*Department of Chemistry, National Tsing Hua University, Hsinchu 300, Taiwan, and* [‡]*Department of Chemistry, National Taiwan University, Taipei 106, Taiwan*

Received March 30, 2009

Sequential treatment of $IrCl_3 \cdot nH_2O$ with 2 equiv of benzyl diphenylphosphine (bdpH) and then 1 equiv of 3-trifluoromethyl-5-(2-pyridyl) pyrazole (fppzH) in 2-methoxyethanol gave formation to three isomeric complexes with formula [Ir(bdp)(fppz)(bdpH)H] (**1**−**3**). Their molecular structures were established by single crystal X-ray diffraction studies, showing existence of one monodentate phosphine bdpH, one terminal hydride, a cyclometalated bdp chelate, and a fppz chelate. Variation of the metal−ligand bond distances showed good agreement with those predicted by the *trans* effect. Raman spectroscopic analyses and the corresponding photophysical data are also recorded and compared. Among all isomers complex **1** showed the worst emission efficiency, while complexes **2** and **3** exhibited the greatest luminescent efficiency in solid state and in degassed CH_2Cl_2 solution at room temperature, respectively. This structural relationship could be due to the simultaneously weakened hydride and the monodentate bdpH bonding that are destabilized by the *trans*-pyrazolate anion and cyclometalated benzyl group, respectively.

1. Introduction

The use of heavy transition metal complexes as emitting materials in organic light-emitting devices (OLEDs), particularly the metal complexes with a Ru(II),[1] Os(II),[2] Ir(III),[3] and Pt(II)[4] central cation, is an area of increasing importance and significance. Among these emitting materials, Ir(III)-containing materials are the most pursued subjects.[5] This interest is motivated by their great emission efficiency, less aggregation in solid state, and improved thermal stabilities. However, a limiting factor of their application in OLEDs is how to conduct the tuning of emission color across the whole visible spectrum. Such perspective has then motivated scientists to investigate the red and green-emitting Ir(III) complexes, for which vast technological progresses have been made. However, among emitting materials that could afford the required Red-Green-Blue (RGB) colors, the true-blue

*To whom correspondence should be addressed. E-mail: ychi@mx.nthu.edu.tw (Y.C.), chop@ntu.edu.tw (P.-T.C.).

(1) (a) Baranoff, E.; Collin, J.-P.; Flamigni, L.; Sauvage, J.-P. *Chem. Soc. Rev*. **2004**, *33*, 147. (b) Tung, Y.-L.; Lee, S.-W.; Chi, Y.; Chen, L.-S.; Shu, C.-F.; Wu, F.-I.; Carty, A. J.; Chou, P.-T.; Peng, S.-M.; Lee, G.-H. *Adv. Mater*. **2005**, *17*, 1059. (c) Tung, Y.-L.; Chen, L.-S.; Chi, Y.; Chou, P.-T.; Cheng, Y.-M.; Li, E. Y.; Lee, G.-H.; Shu, C.-F.; Wu, F.-I.; Carty, A. J. *Adv. Funct. Mater*. **2006**, *16*, 1615.
(2) (a) Chi, Y.; Chou, P.-T. *Chem. Soc. Rev*. **2007**, *36*, 1421. (b) Chou, P.-T.; Chi, Y. *Eur. J. Inorg. Chem*. **2006**, 3319.
(3) (a) Holder, E.; Langeveld, B. M. W.; Schubert, U. S. *Adv. Mater*. **2005**, *17*, 1109. (b) Flamigni, L.; Barbieri, A.; Sabatini, C.; Ventura, B.; Barigelletti, F. *Top. Curr. Chem*. **2007**, *281*, 143. (c) Burn, P. L.; Lo, S.-C.; Samuel, I. D. W. *Adv. Mater*. **2007**, *19*, 1675. (d) Ragni, R.; Orselli, E.; Kottas, G. S.; Omar, O. H.; Babudri, F.; Pedone, A.; Naso, F.; Farinola, G. M.; De Cola, L. *Chem.—Eur. J*. **2009**, *15*, 136.
(4) (a) Lai, S.-W.; Che, C.-M. *Top. Curr. Chem*. **2004**, *241*, 27. (b) Williams, J. A. G.; Wilkinson, A. J.; Whittle, V. L. *Dalton Trans*. **2008**, 2081.
(5) (a) Evans, R. C.; Douglas, P.; Winscom, C. J. *Coord. Chem. Rev*. **2006**, *250*, 2093. (b) You, Y.; Park, S. Y. *Dalton Trans*. **2009**, 1267.
(6) (a) Chang, C.-J.; Yang, C.-H.; Chen, K.; Chi, Y.; Shu, C.-F.; Ho, M.-L.; Yeh, Y.-S.; Chou, P.-T. *Dalton Trans*. **2007**, 1881. (b) Chou, P.-T.; Chi, Y. *Chem.—Eur. J*. **2007**, *13*, 380. (c) Chen, L.; You, H.; Yang, C.; Ma, D.; Qin, J. *Chem. Commun*. **2007**, 1352. (d) You, Y.; Seo, J.; Kim, S. H.; Kim, K. S.; Ahn, T. K.; Kim, D.; Park, S. Y. *Inorg. Chem*. **2008**, *47*, 1476.
(7) (a) Lo, S.-C.; Richards, G. J.; Markham, J. P. J.; Namdas, E. B.; Sharma, S.; Burn, P. L.; Samuel, I. D. W. *Adv. Funct. Mater*. **2005**, *15*, 1451. (b) Yeh, S.-J.; Wu, M.-F.; Chen, C.-T.; Song, Y.-H.; Chi, Y.; Ho, M.-H.; Hsu, S.-F.; Chen, C. H. *Adv. Mater*. **2005**, *17*, 285. (c) Avilov, I.; Minoofar, P.; Cornil, J.; De Cola, L. *J. Am. Chem. Soc*. **2007**, *129*, 8247. (d) Shih, P.-I.; Chien, C.-H.; Chuang, C.-Y.; Shu, C.-F.; Yang, C.-H.; Chen, J.-H.; Chi, Y. *J. Mater. Chem*. **2007**, *17*, 1692. (e) Kwon, T.-H.; Kim, M. K.; Kwon, J.; Shin, D.-Y.; Park, S. J.; Lee, C.-L.; Kim, J.-J.; Hong, J.-I. *Chem. Mater*. **2007**, *19*, 3673. (f) Wu, M.-F.; Yeh, S.-J.; Chen, C.-T.; Murayama, H.; Tsuboi, T.; Li, W.-S.; Chao, I.; Liu, S.-W.; Wang, J.-K. *Adv. Funct. Mater*. **2007**, *17*, 1887. (g) Su, S.-J.; Sasabe, H.; Takeda, T.; Kido, J. *Chem. Mater*. **2008**, *20*, 1691. (h) Orselli, E.; Albuquerque, R. Q.; Fransen, P. M.; Froehlich, R.; Janssen, H. M.; De Cola, L. *J. Mater. Chem*. **2008**, *18*, 4579. (i) Wang, Y.-M.; Teng, F.; Gan, L.-H.; Liu, H.-M.; Zhang, X.-H.; Fu, W.-F.; Wang, Y.-S.; Xu, X.-R. *J. Phys. Chem. C* **2008**, *112*, 4743. (j) Yang, L.; Okuda, F.; Kobayashi, K.; Nozaki, K.; Tanabe, Y.; Ishii, Y.; Haga, M. *Inorg. Chem*. **2008**, *47*, 7154. (k) Stagni, S.; Colella, S.; Palazzi, A.; Valenti, G.; Zacchini, S.; Paolucci, F.; Marcaccio, M.; Albuquerque, R. Q.; De Cola, L. *Inorg. Chem*. **2008**, *47*, 10509. (l) Gu, X.; Fei, T.; Zhang, H.; Xu, H.; Yang, B.; Ma, Y.; Liu, X. *J. Phys. Chem. A* **2008**, *112*, 8387.

Published on Web 08/11/2009

phosphor represents the most difficult one to achieve. This is mainly because it requires the highest excitation energy with the shortest-wavelength phosphorescence output,[6] and thus is commonly subject to the inferiority of weak luminescence yield, incorrect monochromaticity, and short lifespan.

So far, there is an increasing amount of research reporting on how to prepare blue-phosphors and investigate their photophysical and device properties.[7] Thus, having the capability to obtain the true-blue phosphors with good color chromaticity and excellent quantum efficiency would be considered as one important breakthrough in OLEDs. In this paper, we disclosed a new design concept via incorporation of pyridyl azolate chelate, terminal hydride, monodentate and cyclometalated phosphine chelate,[8] giving successful preparation of three isomeric, blue-emitting phosphorescent complexes **1**−**3**. Since neither phosphine ligand nor terminal hydride possesses lower lying π-molecular orbitals and lone pair electrons, both S_1 and T_1 states involved in these Ir(III) complexes are mainly localized at the chelating pyridyl pyrazolate site, and the corresponding S_0-T_1 transition resides within the higher energy region of the visible spectra. Amid this study, an intriguing relationship for structure versus phosphorescent signal intensity was explored, which may have significant implications in the future design and preparation of efficient true blue phosphors. Details of results and discussion are elaborated in the following sections.

2. Experimental Section

General Information and Materials. All reactions were performed under a nitrogen atmosphere using anhydrous solvents or solvents treated with an appropriate drying reagent. Mass spectra were obtained on a JEOL SX-102A instrument operating in electron impact (EI) mode or fast atom bombardment (FAB) mode. ^{1}H and ^{19}F NMR spectra were recorded on Varian Mercury-400 or INOVA-500 instruments. Elemental analyses were conducted at the NSC Regional Instrumentation Center at National Chiao Tung University.

Spectral and Dynamic Measurement. Steady-state absorption and emission spectra were recorded by a Hitachi (U-3310) spectrophotometer and an Edinburgh (FS920) fluorimeter, respectively. Emission quantum yields were measured at excitation wavelength $\lambda_{ex} = 350$ nm in CH_2Cl_2 at room temperature (RT). In this approach, Quinine sulfate with an emission yield of $\Phi \sim 0.54 \pm 0.2$ in 1.0 N sulfuric acid solution served as the standard to calculate the emission quantum yield. A configuration of front-face excitation was used to measure the emission of the solid sample **1**−**3**. The solid sample was fixed by assembling two edge-polished quartz plates with various Teflon spacers. A combination of appropriate filters was used to avoid the interference from the scattering light. An integrating sphere was applied to measure the quantum yield in the solid state, in which the solid film of **1**−**3** was prepared via the spin coating method and was excited by a 325 nm He−Cd laser line. The resulting luminescence was acquired by an intensified charge-coupled detector for subsequent quantum yield analyses. Lifetime studies were performed by an Edinburgh FL 900 photon counting system with a hydrogen-filled or a nitrogen lamp as the excitation source. Data were analyzed using a nonlinear least-squares procedure in combination with an iterative convolution method. Emission decays were analyzed by the sum of exponential functions, which allows partial removal of the instrument time broadening and consequently renders a temporal resolution of ~200 ps.

Confocal Raman spectra of each sample were recorded from their single crystallines and obtained with a Thermo Nicolet Almega XR Dispersive Raman Spectrometer ($\lambda_{ex} = 780$ nm) and a Olympus BX51 Microscope. The measurements were performed with 2 s exposure time, and all spectra were accumulated over an average of 30 scans.

Synthesis of $IrCl_3(THT)_3$. The synthetic protocol was according to a literature report with a slight modification;[9] a mixture of $IrCl_3 \cdot 3H_2O$ (200 mg, 0.57 mmol) and tetrahydrothiophene (THT, 0.25 mL, 2.84 mmol) in 2-methoxyethanol (20 mL) was refluxed for 12 h. After removal of solvent in vacuo, the yellow powder was triturated with a 1:1 mixture of ethyl acetate and hexane, and collected by filtration (271 mg, 0.49 mmol, 85%).

Spectra data of $IrCl_3(THT)_3$. MS (FAB): m/z 562 (M^+). ^{1}H NMR (400 MHz, $CDCl_3$, 294 K): δ 3.64−3.58 (m, 4H), 3.23−3.17 (m, 2H), 2.91−2.80 (m, 6H), 2.30−2.01 (m, 12H).

Synthesis of A. A 50 mL reaction flask was charged with $Ir(THT)_3Cl_3$ (168 mg, 0.3 mmol), benzyldiphenylphosphine (bdpH, 171 mg, 0.62 mmol) and 5-pyridyl-3-trifluoromethyl-1*H*-pyrazole (fppzH, 64 mg, 0.3 mmol). To this mixture degassed decalin (20 mL) was added as solvent. The solution was first refluxed for 1 h. After that, Na_2CO_3 (318 mg, 3.00 mmol) was added, and the mixture was brought to reflux for another 24 h to ensure the complete reaction. Purification was conducted by silica-gel column chromatography eluting with a mixture of ethyl acetate and hexane (1:3) with $R_f = 0.62$. Crystallization from a mixture of ethyl acetate and hexane gave colorless needles of **A** (86 mg, 0.09 mmol, 35%).

Spectral Data of A. MS (FAB, ^{193}Ir): m/z 956 $(M+1)^+$; ^{1}H NMR (500 MHz, $CDCl_3$, 294 K): δ 7.89 (d, $J = 8.0$ Hz, 1H), 7.87 (t, $J = 8.0$ Hz, 1H), 7.50 (d, $J = 6.5$ Hz, 1H), 7.43 (t, $J = 9.0$ Hz, 2H), 7.33−7.25 (m, 3H), 7.21 (d, $J = 7.5$ Hz, 1H), 7.15 (t, $J = 8.0$ Hz, 3H), 7.11−7.08 (m, 5H), 6.96 (t, $J = 7.5$ Hz, 1H), 6.85 (t, $J = 7.5$ Hz, 1H), 6.82−6.79 (m, 3H), 6.77 (s, 1H), 6.72 (t, $J = 7.5$ Hz, 1H), 6.69−6.66 (m, 3H), 6.61 (t, $J = 9.0$ Hz, 2H), 6.43 (t, $J = 7.0$ Hz, 1H), 6.32 (t, $J = 8.5$ Hz, 2H), 6.18 (t, $J = 6.0$ Hz, 1H), 4.05 (dd, $J = 15.0$, 11.0 Hz, 1H), 3.77 (dd, $J = 15.0$, 11.0 Hz, 1H), 3.46 (dd, $J = 16.5$, 10.0 Hz, 1H), 2.17 (dd, $J = 16.5$, 10.0 Hz, 1H); ^{19}F−{^{1}H} NMR (470 MHz, $CDCl_3$, 294 K): δ −60.27 (s, 3F); ^{31}P−{^{1}H} NMR (202 MHz, $CDCl_3$, 294 K): δ 6.29 (d, $J_{PP} = 11$ Hz, 1P), 6.18 (d, $J_{PP} = 11$ Hz, 1P). Anal. Calcd for $C_{47}H_{37}F_3IrN_3P_2$: N, 4.40; C, 59.11; H, 3.91. Found: N, 4.39; C, 58.90; H, 4.09.

Synthesis of Hydride Complexes 1−**3**. A 50 mL reaction flask was first charged with $IrCl_3 \cdot H_2O$ (212 mg, 0.60 mmol) and bdpH (350 mg, 1.26 mmol). To this mixture degassed 2-methoxyethanol (30 mL) was added as solvent. The solution was then refluxed for 12 h and then cooled to ambient. After then, fppzH (128 mg, 0.6 mmol) and Na_2CO_3 (630 mg, 6.00 mmol) were added. The mixture was brought to reflux for another 1 h. After cooling to RT, addition of excess of deionized water resulted in a white precipitate, which was collected by filtration, washed with cold methanol and diethyl ether in sequence. Further purification was conducted by silica-gel column chromatography eluting with a mixture of ethyl acetate and hexane (1:5) with R_f values of complexes **1**, **2**, and **3** being 0.43, 0.16, and 0.57, respectively. All crystalline materials were obtained from a layered solution of CH_2Cl_2 and hexane at RT and were colorless; cf. **1** (84 mg, 0.09 mmol, 15%), **2** (153 mg, 0.16 mmol, 26%), and **3** (57 mg, 0.06 mmol, 10%).

Spectral Data of 1. MS (FAB, ^{193}Ir): m/z 956 $(M-1)^+$; ^{1}H NMR (500 MHz, $CDCl_3$, 294 K): δ 8.40 (t, $J = 7.5$ Hz, 1H), 8.16 (t, $J = 9.0$ Hz, 2H), 7.93−7.89 (m, 2H), 7.48 (t, $J = 7.5$ Hz, 1H), 7.35−7.28 (m, 6H), 7.20 (t, $J = 7.5$ Hz, 1H), 7.07 (t, $J = 8.5$ Hz, 2H), 7.01−6.98 (m, 3H), 6.92 (d, $J = 7.5$ Hz, 1H), 6.87

(8) Chiu, Y.-C.; Hung, J.-Y.; Chi, Y.; Chen, C.-C.; Chang, C.-H.; Wu, C.-C.; Cheng, Y.-M.; Yu, Y.-C.; Lee, G.-H.; Chou, P.-T. *Adv. Mater.* **2009**, *21*, 2221.

(9) John, D.; Salazar, K. V.; Scott, B. L.; Baker, R. T.; Sattelberger, A. P. *Organometallics* **2001**, *20*, 296.

Table 1. Crystal Data and Structure Refinement Parameters for Complexes **1**, **2**, and **3**

complex	**1**	**2**·0.75 × CH_2Cl_2·0.5 × H_2O	**3**
empirical formula	$C_{47}H_{39}F_3IrN_3P_2$	$C_{47.75}H_{41.50}Cl_{1.50}F_3IrN_3O_{0.50}P_2$	$C_{47}H_{39}F_3IrN_3P_2$
formula weight	956.95	1029.65	956.95
temperature	150(2) K	150(2) K	150(2) K
crystal system	triclinic	triclinic	monoclinic
space group	$P\bar{1}$	$P\bar{1}$	$P2_1/c$
a	12.3595(8) Å	13.3687(6) Å	14.6300(6) Å
b	13.3107(8) Å	18.0579(8) Å	14.9847(6) Å
c	13.7068(8) Å	19.5186(9) Å	18.2547(8) Å
α	75.969(1)°	100.571(1)°	
β	69.893(1)°	100.911(1)°	92.581(1)°
γ	74.047(1)°	104.355(1)°	
volume, *Z*	2008.4(2) $Å^3$, 2	4348.9(3) $Å^3$, 4	3997.8(3) $Å^3$, 4
density (calculated)	1.582 Mg/m^3	1.573 Mg/m^3	1.590 Mg/m^3
absorption coefficient	3.455 mm^{-1}	3.287 mm^{-1}	3.472 mm^{-1}
F(000)	952	2050	1904
crystal size (mm^3)	0.30 × 0.12 × 0.12	0.22 × 0.12 × 0.05	0.24 × 0.15 × 0.15
reflections collected	26147	47094	30448
independent reflections	9195 [*R*(int) = 0.0284]	15332 [*R*(int) = 0.0654]	9183 [*R*(int) = 0.0388]
max. and min transmission	0.6819 and 0.4238	0.8529 and 0.5316	0.6240 and 0.4896
data /restraints /parameters	9195/0/521	15332/2/1050	9183/0/535
Goodness-of-fit on F^2	1.036	1.079	1.110
final *R* indices [$I \geq 2\sigma(I)$]	R1 = 0.0236, wR2 = 0.0553	R1 = 0.0531, wR2 = 0.1092	R1 = 0.0318, wR2 = 0.0645
R indices (all data)	R1 = 0.0262, wR2 = 0.0563	R1 = 0.0671, wR2 = 0.1167	R1 = 0.0375, wR2 = 0.0665
largest diff. peak and hole	1.164 and −0.668 e/$Å^3$	1.725 and −1.723 e/$Å^3$	1.042 and −1.041 e/$Å^3$

(t, J = 7.5 Hz, 1H), 6.76−6.72 (m, 4H), 6.63 (s, 1H), 6.62−6.44 (m, 7H), 6.07 (d, J = 8.0 Hz, 2H), 5.16 (dd, J = 15.0, 11.0 Hz, 1H), 3.69 (t, J = 15.0 Hz, 1H), 2.96 (dd, J = 15.0, 6.0 Hz, 1H), 2.88 (dd, J = 15.0, 6.0 Hz, 1H), −17.84 (dd, J = 17.5, 14.5 Hz, 1H). ^{19}F-{^1H} NMR (470 MHz, $CDCl_3$, 294 K): δ −60.04 (s, 3F). ^{31}P-{^1H} NMR (202 MHz, $CDCl_3$, 294 K): δ 20.05 (d, J_{PP} = 11.1 Hz, 1P), 4.09 (d, J_{PP} = 11.1 Hz, 1P). Anal. Calcd for $C_{47}H_{39}F_3IrN_3P_2$: N, 4.39; C, 58.99; H, 4.11. Found: N, 4.36; C, 58.66; H, 4.40

Spectral Data of 2. MS (FAB, ^{193}Ir): m/z 957 (M^+); ^1H NMR (500 MHz, $CDCl_3$, 294 K): δ 7.60−7.50 (m, 6H), 7.36 (t, J = 7.0 Hz, 1H), 7.29 (t, J = 7.0 Hz, 1H), 7.23−7.20 (m, 2H), 7.15−7.05 (m, 6H), 6.99−6.95 (m, 3H), 6.93 (s, 1H), 6.80 (t, J = 8.0 Hz, 1H), 6.76 (t, J = 7.0 Hz, 1H), 6.68−6.62 (m, 3H), 6.69 (d, J = 5.5 Hz, 1H), 6.53 (t, J = 8.5 Hz, 2H), 6.44−6.39 (m, 3H), 6.23 (dd, J = 8.0, 5.0 Hz, 1H), 6.03 (d, J = 8.5 Hz, 2H), 4.01 (dd, J = 16.0, 11.0 Hz, 1H), 3.35 (dd, J = 16.0, 11.0 Hz, 1H), 2.67 (dd, J = 14.5, 5.0 Hz, 1H), 2.13 (dd, J = 14.5, 5.0 Hz, 1H), −19.31 (dd, J = 25.5, 11.0 Hz, 1H). ^{19}F-{^1H} NMR (470 MHz, $CDCl_3$, 294 K): δ −60.08 (s, 3F). ^{31}P-{^1H} NMR (202 MHz, $CDCl_3$, 294 K): δ 18.65 (d, J_{PP} = 11.1 Hz, 1P), 4.15 (d, J_{PP} = 11.1 Hz, 1P). Anal. Calcd for $C_{47}H_{39}F_3IrN_3P_2$: N, 4.39; C, 58.99; H, 4.11. Found: N, 4.35; C, 59.12; H, 4.52.

Spectral Data of 3. MS (FAB, ^{193}Ir): m/z 957 (M^+); ^1H NMR (500 MHz, $CDCl_3$, 294 K): δ 8.00−7.89 (m, 2H), 7.41−7.39 (m, 3H), 7.26 (d, J = 6.5 Hz, 1H), 7.21 (t, J = 7.5 Hz, 2H), 7.11 (t, J = 7.5 Hz, 1H), 7.05−7.01 (m, 3H), 7.00−6.97 (m, 5H), 6.92−6.86 (m, 6H), 6.81 (t, J = 7.5 Hz, 1H), 6.79 (t, J = 7.0 Hz, 1H), 6.73−6.72 (m, 3H), 6.66 (t, J = 7.0 Hz, 2H), 6.45−6.40 (m, 3H), 6.06 (t, J = 6.0 Hz, 1H), 4.06 (t, J = 14.0 Hz, 1H), 3.90 (dd, J = 14.5, 8.5 Hz, 1H), 3.57 (dd, J = 14.5, 8.5 Hz, 1H), 3.28 (t, J = 14.0 Hz, 1H), −18.86 (t, J = 17.6 Hz, 1H). ^{19}F-{^1H} NMR (470 MHz, $CDCl_3$, 294 K): δ −60.04 (s, 3F). ^{31}P-{^1H} NMR (202 MHz, $CDCl_3$, 294 K): δ 23.58 (d, J_{PP} = 369 Hz, 1P), 13.38 (d, J_{PP} = 369 Hz, 1P). Anal. Calcd for $C_{47}H_{39}F_3IrN_3P_2$: N, 4.39; C, 58.99; H, 4.11. Found: N, 4.45; C, 58.87; H, 4.40.

X-ray Diffraction Studies. Single crystal X-ray diffraction data of **1**, **2**, and **3** were measured on a Bruker SMART Apex CCD diffractometer using (Mo Kα) radiation (λ = 0.71073 Å). The data collection was executed using the SMART program. The hydride of each complexes was located in the difference Fourier and refined independently. Cell refinement and data reduction were performed with the SAINT program. The structure was determined using the SHELXTL/PC program and refined using full-matrix least-squares (Table 1). The crystalline sample of **3** crystallized with 3 equiv of CH_2Cl_2 and 1 equiv of H_2O in the unit cell.

Computational Methodology. Geometry optimization of the singlet ground state (S_0) and lowest-lying triplet excited state (T_1) were performed using the density functional theory (DFT) at the B3LYP level.[10] Restricted and unrestricted formalisms were adopted in the singlet and triplet geometry optimization calculations, respectively. The 6-31G(d) basis set was employed for H, C, N, F atoms and a double-ξ quality basis set, LANL2DZ,[11] consisting of Hay and Wadt's effective core potentials (ECP), was employed for the Ir atom. Furthermore, vibrational frequencies were then calculated based on the optimized ground and lowest triplet state geometries of all complexes to verify that each of the structures is at its global minimum. Calculated Ir−H stretching frequency of the titled complexes compared to the experimental Raman spectral results were also shown in the Results and Discussion section.

To gain better insight into the nature of spectroscopic properties, time dependent DFT (TD-DFT) calculations[12] were executed employing the optimized geometries at the lowest singlet and triplet states, and then applied to probe the absorption and emission properties. Typically, the lowest triplet and 10 singlet roots of the non-hermitian eigenvalue equations were obtained to determine the vertical excitation energies. Oscillator strengths were deduced from the dipole transition matrix elements (for singlet states only). All calculations were carried out using Gaussian 03.[13]

(10) (a) Lee, C.; Yang, W.; Parr, R. G. *Phys. Rev. B* **1988**, *37*, 785. (b) Becke, A. D. *J. Chem. Phys.* **1993**, *98*, 5648.

(11) (a) Hay, P. J.; Wadt, W. R. *J. Chem. Phys.* **1985**, *82*, 270. (b) Wadt, W. R.; Hay, P. J. *J. Chem. Phys.* **1985**, *82*, 284. (c) Hay, P. J.; Wadt, W. R. *J. Chem. Phys.* **1985**, *82*, 299.

(12) (a) Jamorski, C.; Casida, M. E.; Salahub, D. R. *J. Chem. Phys.* **1996**, *104*, 5134. (b) Petersilka, M.; Grossmann, U. J.; Gross, E. K. U. *Phys. Rev. Lett.* **1996**, *76*, 1212. (c) Bauernschmitt, R.; Ahlrichs, R.; Hennrich, F. H.; Kappes, M. M. *J. Am. Chem. Soc.* **1998**, *120*, 5052. (d) Casida, M. E. *J. Chem. Phys.* **1998**, *108*, 4439. (e) Stratmann, R. E.; Scuseria, G. E.; Frisch, M. J. *J. Chem. Phys.* **1998**, *109*, 8218.

(13) *Gaussian 03*, revision C.02; Gaussian, Inc.: Wallingford, CT, 2004.

Compositions of molecular orbitals in terms of the constituent chemical fragments were calculated using the AOMix program.[14] For the characterization of the HOMO−x → LUMO+y transitions as partial charge transfer (CT) transitions, the following definition of the CT character has been used:

$$\mathrm{CT(M)} = \%\mathrm{(M)HOMO{-}x} - \%\mathrm{(M)LUMO{+}y}$$

where %(M)HOMO−x and %(M)LUMO+y are electronic densities on the metal in HOMO−x and LUMO+y. If the excited state, for example, S_1 or T_1, is formed by more than one one-electron excitation, then the metal CT character of this excited state is expressed as a sum of CT characters of each participating excitation, $i \rightarrow j$:

$$\mathrm{CT_I(M)} = \sum_{i,\mathrm{a}} [\mathrm{C_I}(i \rightarrow j)]^2 (\%(\mathrm{M})_i - \%(\mathrm{M})_j)$$

where $C_I(i \rightarrow j)$ are the appropriate coefficients of the I-th eigenvector of the CI matrix. Accordingly, one can very effectively use the MO compositions in terms of fragment orbital contributions to analyze the nature of electronic transitions.

3. Results and Discussion

Traditionally, the blue phosphorescent transition metal complexes were synthesized employing a wide-energy-gap cyclometalated ligand, such as 4,6-difluorophenyl pyridine (dfppyH),[15] and the respective functionalized cyclometalates.[16] It is believed that, upon forming metal complexes, as the electron withdrawing fluoro substituents are located at the *meta*-positions with respect to the central metal atom, a larger stabilization of the metal d_π orbitals is expected. On the other hand, since these fluoro substituents are also located at the *ortho* and *para* position relative to the pyridyl group, it is doubtless that the resonance (mesomeric) effects would exert an opposite influence to the anticipated inductive effect,[17] giving a much reduced influence on the energy level of the adjacent pyridyl π^* orbital, and hence manifesting excessive ligand-centered $\pi\pi^*$ energy required for blue phosphorescence. Although such properties have not been explicitly elaborated in literature,[18] the respective dfppy chelates have been successfully utilized for preparation of numerous blue phosphorescent complexes by taking advantage of its higher lying π^* orbital on the pyridyl segment.[19]

To move on one more step, because of their multisubstituted nitrogen atoms at the azolate site and the CF_3 substituent, 2-pyridyl azoles, such as 3-trifluoromethyl-5-(2-pyridyl) pyrazole (fppzH) and its analogues, are expected to offer an even wider $\pi\pi^*$ energy gap than dfppyH. Examples for high efficiency, true-blue phosphorescent materials have been demonstrated in the Os(II) complexes known as $[Os(fppz)_2(CO)_2]$,[20] $[Os(CO)_3(tfa)(fppz)]$, tfa = trifluoroacetate, and analogues[21] in our recent studies. Subsequently, we also synthesized a class of heteroleptic Ir(III) complexes assembled using both fppz chromophore and non-chromophoric, ancillary chelates with an excessively large ligand-centered $\pi\pi^*$ energy gap.[6a] Depending on the intrinsic characteristics of the non-chromophoric ligands, RT true-blue phosphorescence was noted in both fluid and solid states;[22] for example, the stronger ligand field strength, non-conjugated ancillary chelates are found to be capable of inducing the light output from the aforementioned fppz chelate with little loss of its emission efficiency.[8,23]

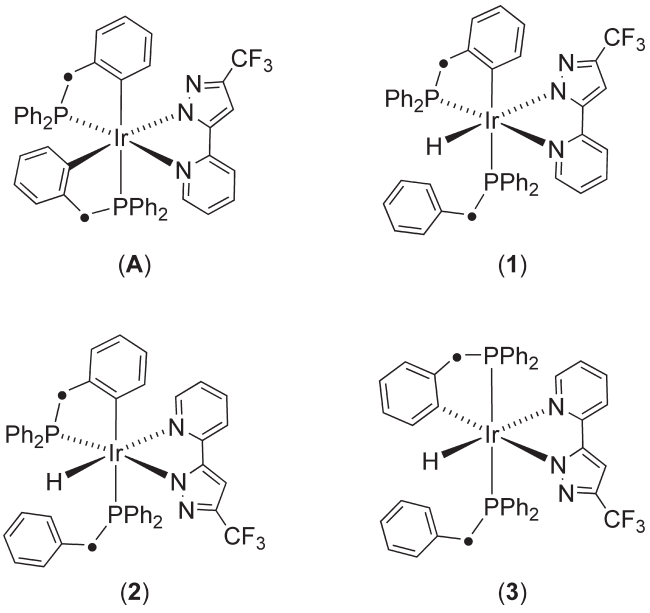

With these precedent experiences in mind, we then carried out the reaction of $IrCl_3 \cdot nH_2O$ with 2 equiv of benzyldiphenylphosphine (bdpH) in 2-methoxyethanol, followed by treatment with the aforementioned fppzH ligand in the presence of Na_2CO_3. Our strategy was to allow a prior coordination of bdpH ligands to the Ir(III) metal center, affording an Ir(III)

(14) (a) Gorelsky, S. I. *AOMix: Program for Molecular Orbital Analysis*; University of Ottawa: Ottawa, Ontario, Canada, 2007; http://www.sg-chem.net/. (b) Gorelsky, S. I.; Lever, A. B. P. *J. Organomet. Chem.* **2001**, *635*, 187.

(15) Li, J.; Djurovich, P. I.; Alleyne, B. D.; Tsyba, I.; Ho, N. N.; Bau, R.; Thompson, M. E. *Polyhedron* **2004**, *23*, 419.

(16) (a) Lo, S.-C.; Shipley, C. P.; Bera, R. N.; Harding, R. E.; Cowley, A. R.; Burn, P. L.; Samuel, I. D. W. *Chem. Mater.* **2006**, *18*, 5119. (b) Lee, S. J.; Park, K.-M.; Yang, K.; Kang, Y. *Inorg. Chem.* **2009**, *48*, 1030.

(17) (a) Cheng, Y.-M.; Yeh, Y.-S.; Ho, M.-L.; Chou, P.-T.; Chen, P.-S.; Chi, Y. *Inorg. Chem.* **2005**, *44*, 4594. (b) Hwang, K.-C.; Chen, J.-L.; Chi, Y.; Lin, C.-W.; Cheng, Y.-M.; Lee, G.-H.; Chou, P.-T.; Lin, S.-Y.; Shu, C.-F. *Inorg. Chem.* **2008**, *47*, 3307.

(18) Nazeeruddin, M. K.; Gratzel, M. *Struct. Bonding* (*Berlin*) **2007**, *123*, 113.

(19) (a) Coppo, P.; Plummer, E. A.; De Cola, L. *Chem. Commun.* **2004**, 1774. (b) Tamayo, A. B.; Alleyne, B. D.; Djurovich, P. I.; Lamansky, S.; Tsyba, I.; Ho, N. N.; Bau, R.; Thompson, M. E. *J. Am. Chem. Soc.* **2003**, *125*, 7377. (b) Wu, L.-L.; Yang, C.-H.; Sun, I.-W.; Chu, S.-Y.; Kao, P.-C.; Huang, H.-H. *Organometallics* **2007**, *26*, 2017. (c) Yang, C.-H.; Cheng, Y.-M.; Chi, Y.; Hsu, C.-J.; Fang, F.-C.; Wong, K.-T.; Chou, P.-T.; Chang, C.-H.; Tsai, M.-H.; Wu, C.-C. *Angew. Chem., Int. Ed.* **2007**, *46*, 2418. (d) De Angelis, F.; Fantacci, S.; Evans, N.; Klein, C.; Zakeeruddin, S. M.; Moser, J.-E.; Kalyanasundaram, K.; Bolink, H. J.; Graetzel, M.; Nazeeruddin, M. K. *Inorg. Chem.* **2007**, *46*, 5989. (e) He, L.; Duan, L.; Qiao, J.; Wang, R.; Wei, P.; Wang, L.; Qiu, Y. *Adv. Funct. Mater.* **2008**, *18*, 2123. (f) Di Censo, D.; Fantacci, S.; De Angelis, F.; Klein, C.; Evans, N.; Kalyanasundaram, K.; Bolink, H. J.; Graetzel, M.; Nazeeruddin, M. K. *Inorg. Chem.* **2008**, *47*, 980.

(20) (a) Wu, P.-C.; Yu, J.-K.; Song, Y.-H.; Chi, Y.; Chou, P.-T.; Peng, S.-M.; Lee, G.-H. *Organometallics* **2003**, *22*, 4938. (b) Yu, J.-K.; Hu, Y.-H.; Cheng, Y.-M.; Chou, P.-T.; Peng, S.-M.; Lee, G.-H.; Carty, A. J.; Tung, Y.-L.; Lee, S.-W.; Chi, Y.; Liu, C.-S. *Chem.—Eur. J.* **2004**, *10*, 6255.

(21) Cheng, Y.-M.; Li, E. Y.; Lee, G.-H.; Chou, P.-T.; Lin, S.-Y.; Shu, C.-F.; Hwang, K.-C.; Chen, Y.-L.; Song, Y.-H.; Chi, Y. *Inorg. Chem.* **2007**, *46*, 10276.

(22) Song, Y.-H.; Chiu, Y.-C.; Chi, Y.; Cheng, Y.-M.; Lai, C.-H.; Chou, P.-T.; Wong, K.-T.; Tsai, M.-H.; Wu, C.-C. *Chem.—Eur. J.* **2008**, *14*, 5423.

(23) Chang, C.-F.; Cheng, Y.-M.; Chi, Y.; Chiu, Y.-C.; Lin, C.-C.; Lee, G.-H.; Chou, P.-T.; Chen, C.-C.; Chang, C.-H.; Wu, C.-C. *Angew. Chem., Int. Ed.* **2008**, *47*, 4542.

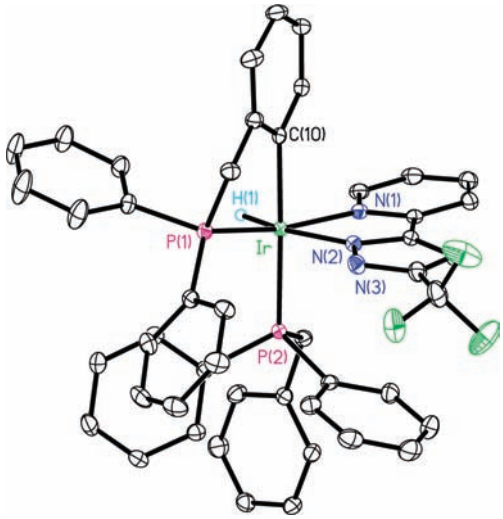

Figure 1. ORTEP diagram of **1** with thermal ellipsoids shown at 30% probability level; selected bond lengths (Å) follow: Ir−C(10) = 2.102(3), Ir−P(1) = 2.2437(7), Ir−P(2) = 2.3303(6), Ir−N(1) = 2.124(2), and Ir−N(2) = 2.107(2) Å; the hydride is shown in the calculated position.

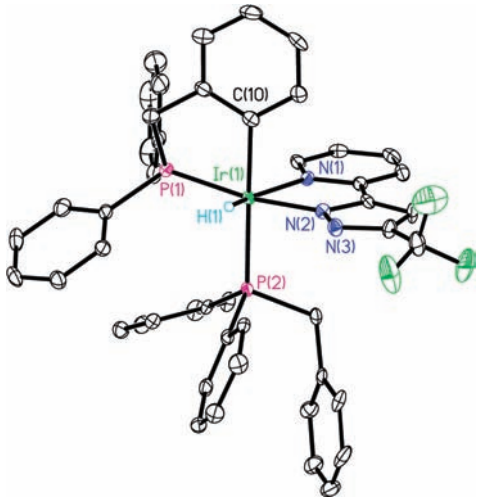

Figure 2. ORTEP diagram of **2** with thermal ellipsoids shown at 30% probability level; selected bond lengths (Å) follow: Ir(1)−C(10) = 2.104(8), Ir(1)−P(1) = 2.247(2), Ir(1)−P(2) = 2.360(2), Ir(1)−N(1) = 2.229(6), and Ir(1)−N(2) = 2.061(7) Å; the hydride is shown in the calculated position.

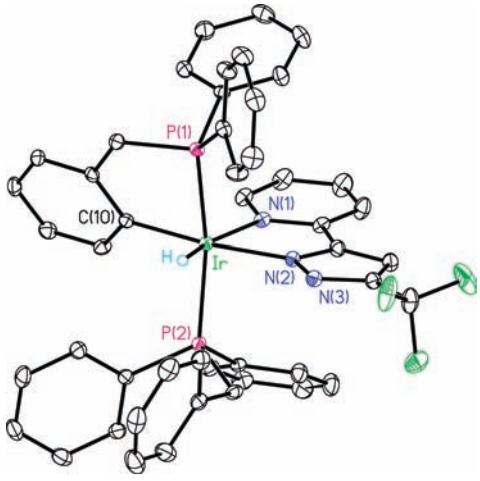

Figure 3. ORTEP diagram of **3** with thermal ellipsoids shown at 30% probability level; selected bond lengths (Å) follow: Ir−C(10) = 2.067(3), Ir−P(1) = 2.2744(9), Ir−P(2) = 2.3168(9), Ir−N(1) = 2.175(3), and Ir−N(2) = 2.110(3) Å; the hydride is shown in the calculated position.

complex with hypothetical formula of $IrCl_3(bdpH)_2$, for which its analogue $IrCl_3(PPh_3)_2$, probably as a 5-coordinate complex in solution, has been independently prepared from reaction of $IrCl(PPh_3)_3$ with chlorine.[24] Afterwards, the phosphine coordination could then facilitate the subsequent cyclometalation at both of the benzyl and relevant sites.[25] The remaining empty coordination site, or sites occupied by either solvent molecule or chlorides, would be substituted by the incoming fppz chelate, giving a proposed Ir(III) complex **A** (see above Scheme) possessing per se three chelating ligands.

However, the reaction did not proceed in accordance with the proposed pathway. Instead, after single cyclometalation, serendipitously, it affords three air stable, isomeric hydride complexes **1**, **2**, and **3** with yields of 15%, 26%, and 10%, respectively. The existence of hydride is unambiguously identified by the ^{1}H NMR signals observed in the range δ −17.84 to −19.31, while their spectral pattern is consistent with the structures in that the hydride is coupled to two strongly coupled, but distinctive, phosphorus nuclei and thus appears as either a doublet of doublet or a triplet in the ^{1}H NMR spectra. The source of hydride has not been confirmed in this reaction, but the 2-methoxyethanol solvent could plausibly be the major supplier, as evidenced by earlier reports on the related Ir(III) system[26] as well as the isoelectronic Os(II) complexes.[27] Finally, to our disappointment, none of these hydride complexes underwent H_2 elimination to afford the proposed target complex, namely, the fully cyclometalated product **A**. Instead, complex **A** was synthesized by treatment of a mixture of dbpH and fppzH with $Ir(THT)_3Cl_3$ in high boiling decalin solvent and then served as a controlled protocol.

Complexes **1**, **2**, and **3** were further characterized through crystal structural analyses. Figures 1, 2, and 3 depict their molecular structures, together with the metric parameters that reveal the systematic variation of bond strengths caused by geometrical isomerism. Salient differences among their X-ray crystal structures are summarized: (i) The monodentate bdpH ligand in all derivatives is found to coordinate to the axial position relative to the square plane defined by the fppz ligand. (ii) The Ir−P(2) distance of monodentate bdpH ligand increases in the order of **3** < **1** < **2** (see Table 2), for which the strongest Ir−P bonding occurred with its *trans*-ligand being switched from Ir−$C_{(benzyl)}$ site to PPh_2 fragment. (iii) The hydride ligands in **1**, **2**, and **3** were located at the *trans* disposition to the pyrazolate N(2), pyridyl N(1), and pyridyl N(1) atom, respectively. Because of the *trans*-effect, the longest Ir−N(1) distance observed in **2** suggested it may possess the strongest Ir−H bonding among all three iridium complexes. (iv) The chelating bdp ligand seems to possess a notably stronger Ir−P bonding interaction compared with the monodentate bdpH ligand. This is revealed by the shortened Ir−P(1) distance in all derivative

(24) Bennett, M. A.; Milner, D. L. *J. Am. Chem. Soc.* **1969**, *91*, 6983.
(25) (a) Verstuyft, A. W.; Redfield, D. A.; Cary, L. W.; Nelson, J. H. *Inorg. Chem.* **1977**, *16*, 2776. (b) Klein, H.-F.; Beck, R.; Florke, U.; Haupt, H.-J. *Eur. J. Inorg. Chem.* **2003**, 853. (c) Frech, C. M.; Leitus, G.; Milstein, D. *Organometallics* **2008**, *27*, 894.
(26) Ionkin, A. S.; Marshall, W. J. *Organometallics* **2004**, *23*, 6031.
(27) (a) Sullivan, B. P.; Caspar, J. V.; Meyer, T. J. *Organometallics* **1984**, *3*, 1241. (b) Hsu, F.-C.; Tung, Y.-L.; Chi, Y.; Hsu, C.-C.; Cheng, Y.-M.; Ho, M.-L.; Chou, P.-T.; Peng, S.-M.; Carty, A. J. *Inorg. Chem.* **2006**, *45*, 10188. (c) Dickinson, P. W.; Girolami, G. S. *Inorg. Chem.* **2006**, *45*, 5215.

Table 2. Selected Bond Lengths (Å) of Ground State Optimized Geometries for Complex **1**−**3**[a]

	Ir−H(1)[b]	Ir−C(10)	Ir−P(1)	Ir−P(2)	Ir−N(1)	Ir−N(2)
1	1.61	2.108 [2.102]	2.307 [2.244]	2.439 [2.330]	2.136 [2.124]	2.171 [2.107]
2	1.58	2.108 [2.105]	2.326 [2.247]	2.431 [2.360]	2.268 [2.229]	2.078 [2.062]
3	1.59	2.098 [2.067]	2.334 [2.274]	2.396 [2.317]	2.243 [2.175]	2.146 [2.110]

[a] The data shown in square bracket are obtained from X-ray diffraction studies. [b] The Ir−H distances obtained from X-ray structural determination were removed because of the poor accuracy.

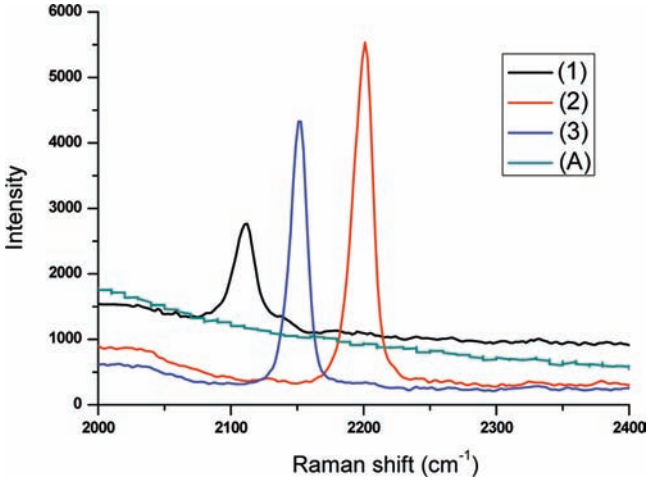

Figure 4. Raman spectra of complexes **A**, **1**, **2**, and **3** in solid in the region of 2000−2400 cm^{-1}.

complexes, as well as those reported in other phosphine substituted Ir(III) derivatives (2.434−2.307 Å).[28] Moreover, even in **3**, where both phosphine fragments are located at the *trans*-disposition, the chelating Ir−P(1) bond is still found to be shortened by 0.0424(9) Å. (v) The Ir−C(10) distances of bdp chelate followed a trend of **1** ∼ **2** > **3**, showing a stronger *trans* effect exerted by the phosphine fragment versus the pyrazolate anion. (vi) The Ir−N(2) distances of the pyrazolate sites followed a sequence of **3** > **1** > **2**. This observation is in good agreement with a better σ-donating effect of the phenyl group versus hydride, as well as a π-accepting effect of phosphine.

As for (iii), because of the weak scattering factors for hydrogen versus nearby iridium, the hydride position could not be exactly located either by difference Fourier or by mean of least-squares refining.[26] Thus, comparison of such structural data is only qualitative and must be treated with extreme caution. To provide further support of the trend of Ir−H bond strengths, both Raman experiments and calculations of corresponding vibrational frequencies of **1**−**3** were performed (see Experimental Section for details). Figure 4 shows the results of Raman spectra for the crystalline samples of **1**−**3**, in which Ir−H stretching frequencies of 2110, 2200, and 2150 cm^{-1} are resolved for complexes **1**, **2**, and **3**, respectively. The assignment of this band is qualitative in accordance with the calculated Ir−H stretching frequencies of 2181 cm^{-1} (**1**), 2254 cm^{-1} (**2**), and 2232 cm^{-1} (**3**). Note that the observed discrepancy, in part, may be attributed to the fact that the experimental and theoretical approach are performed in the solid state and gas phase, respectively. Upon geometry optimization, the Ir−H bond distance is calculated to be 1.61, 1.58, and 1.59 Å (see Table 2) for **1**, **2**, and **3**, respectively, which is not only in line with the ν(Ir−H) bands detected in Raman spectroscopy but also shows good agreement with the anticipated Ir−H distances documented in literature reports.[29] For the controlled experiment, as shown in Figure 4, complex **A** failed to show any vibrational peak at the region between 2000−2400 cm^{-1}, which falls within the typical region expected for ν(Ir−H) bands.[30] Unfortunately, all these hydride complexes **1**−**3** failed to undergo H/D exchange with D_2O or CD_3OD,[31] even in presence of added CF_3CO_2D or NaOD. Thus, confirmation of these Ir−H peaks by classical isotope labeling experiments was not conducted further.

Having proven structural differences among complexes **1**−**3**, we decided to investigate the photophysical properties in an attempt to decipher the factors that govern their, for example, relative emission quantum yield. All pertinent photophysical data are listed in Table 3. Figure 5 depicts the absorption and emission spectra measured in CH_2Cl_2 solution and 77 K cryogenic matrix, while the respective solid state emissions at RT are depicted in Figure 6. In a qualitative manner, their identical spectral profile shown in Figure 5 implicates similar type of transition characteristics for all complexes: The < 300 nm region in the absorption spectra of **1**−**3** all displays an intense ligand-centered $\pi\pi^*$ transition. Subsequently, the absorption bands ranging from 300−400 nm are plausibly attributed to the spin-allowed and/or spin-forbidden MLCT mixed with $\pi\pi^*$ transitions. Additional supports for these assignments are provided in TD-DFT calculation and molecular orbital analyses (vide infra).

All **1**−**3** complexes exhibit true-blue emission peaked centered at around 460 nm in RT CH_2Cl_2. This, in theory, is expectable because of their geometrical isomerism in nature. The luminescence spectra of **2** and **3** reveal clearly the feature of $\pi\pi^*$ vibronic progression. For **1**, because of the much weaker intensity (vide infra), the lack of structural feature for emission in solution may plausibly result from the wide openness of both excitation and emission slits of the fluorimeter. This viewpoint is further supported by the emission spectra acquired in the 77 K CH_2Cl_2 matrixes, in which all three complexes, exhibit strong emissions possessing obvious vibronic fine structure. The radiative lifetime, deduced from the observed lifetime divided by the respective

(28) (a) Li, J.; Djurovich, P. I.; Alleyne, B. D.; Yousufuddin, M.; Ho, N. N.; Thomas, J. C.; Peters, J. C.; Bau, R.; Thompson, M. E. *Inorg. Chem.* **2005**, *44*, 1713. (b) Lyu, Y.-Y.; Byun, Y.; Kwon, O.; Han, E.; Jeon, W. S.; Das, R. R.; Char, K. *J. Phys. Chem. B* **2006**, *110*, 10303. (c) Chin, C. S.; Eum, M.-S.; Kim, S. Y.; Kim, C.; Kang, S. K. *Eur. J. Inorg. Chem.* **2007**, 372.

(29) (a) Salomon, M. A.; Braun, T.; Krossing, I. *Dalton Trans.* **2008**, 5197. (b) Alvarez, E.; Paneque, M.; Petronilho, A. G.; Poveda, M. L.; Santos, L. L.; Carmona, E.; Mereiter, K. *Organometallics* **2007**, *26*, 1231.

(30) (a) Carlo Preti, C.; Tosi, G. *Transition Met. Chem.* **1977**, *2*, 1. (b) Socol, S. M.; Yang, C.; Meek, D. W.; Glaser, R. *Can. J. Chem.* **1992**, *70*, 2424. (c) Albinat, A.; Venanzi, L. M. *Coord. Chem. Rev.* **2000**, *200*−*202*, 687. (d) Acha, F.; Garralda, M. A.; Ibarlucea, L.; Pinilla, E.; Torres, M. R. *Inorg. Chem.* **2005**, *44*, 9084.

(31) Frost, B. J.; Mebi, C. A. *Organometallics* **2004**, *23*, 5317.

Table 3. Photophysical Data of Complexes of **1**−**3** Recorded in CH_2Cl_2 Solution and in Solid State

	λ_{abs}/nm ($\varepsilon \times 10^3$ M^{-1} cm^{-1})	λ_{em}/nm, 298 K, [77 K]	Φ_{em}	τ_{obs} (ns)	τ_{rad} (μs)	k_r[a]	k_{nr}[a]
1	275 (18.9), 320 (9.0), 367 (1.6)	459 [449, 470]	4.0×10^{-4} (5.1×10^{-4})[b]	2.9 (5.2)[b]	7.3 (10.2)	1.3×10^5	3.4×10^8
2	273 (20.2), 325 (8.9)	457 [447, 463]	1.1×10^{-3} (0.62)[b]	10.1 (7100)[b]	9.2 (11.5)	1.0×10^5	9.9×10^7
3	271 (26.4), 316 (7.7), 354 (1.5)	448 [440, 463]	9.7×10^{-3} (0.015)[b]	90.2 (103)[b]	9.3 (6.9)	1.1×10^5	1.1×10^7

[a] k_r (radiative decay rate constant) and k_{nr} (non-radiative decay rate constant) were calculated according to the equations, $k_r = \Phi/\tau_{obs}$ and $k_{nr} = (1/\tau_{obs}) - k_r$. [b] Data measured in solid state.

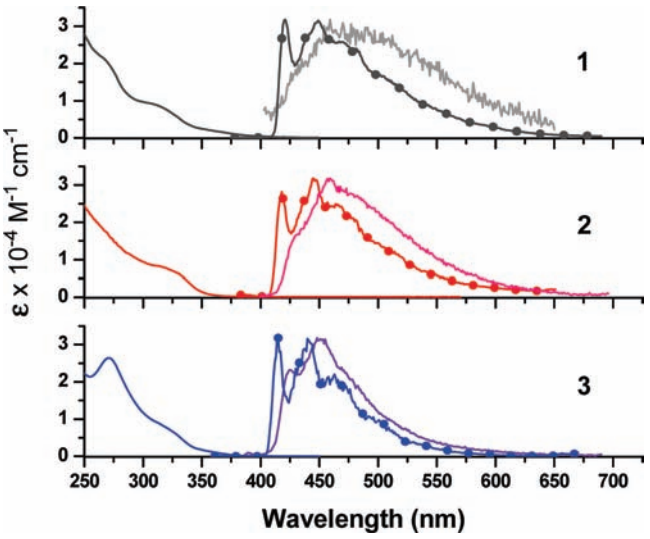

Figure 5. UV/vis absorption and emission spectra of complexes **1**, **2**, and **3** in CH_2Cl_2 solution at 298 K. The solid circle shows the corresponding emission spectra in a 77 K CH_2Cl_2 matrix.

Q.E. in degassed condition, is around ∼10 μs (**1**: 7.3 μs, **2**: 9.2 μs, **3**: 9.3 μs) for all complexes (see Table 3). These results render confirmation that the emission originates from a triplet state manifold with a great percentage of $^3\pi\pi^*$ transition character. Further support of this assignment is given by the fact that the observed spectral profile also showed good agreement with those of the relevant Os(II) complex with formula $[Os(fppz)_2(CO_2)]$.[20] In sharp contrast, the potassium salt of fppz chelate, namely, [(fppz)K], or even the boron metal complex $[B(C_6F_5)_2(fppz)]$ exhibits normal short-lived, fluorescence maximized at 372 and 380 nm, respectively. The results manifest a fast rate of $S_1 \rightarrow T_1$ intersystem crossing enhanced by Ir (or Os) spin−orbit coupling.

Despite the seemingly identical spectral profiles among **1**−**3**, however, drastically different emission intensity was resolved in solution. In terms of emission quantum yield, it ranges from very weak in **1** (4.0×10^{-4}), weak in **2** (1.1×10^{-3}) to moderate intensity (∼0.01) in **3**. The difference in emission intensity goes up to as large as 25 fold between **1** and **3**, which is also clearly shown in the emission appearance viewed with the naked eyes (see Table of Contents (TOC)). We also performed luminescence studies in solid state. As shown in Figure 6 and the TOC illustration, while the solid state emission of **1** is still weak, relatively stronger emission intensity was observed for the solid sample of **2** and **3**. Particularly, as shown in the TOC, **2** exhibits very strong emission in solid. Quantum yield of the titled complexes in solid was then measured to be 5.1×10^{-4}, 0.62 and ∼0.015 for **1**, **2**, and **3**, respectively (see Table 3). Note that the observed lifetime for **2** in solid is measured to be as long as 7.1 μs, firmly supporting its phosphorescence origin.

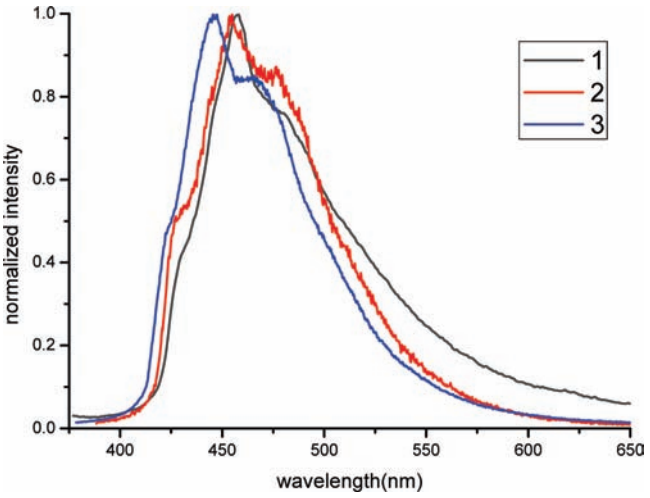

Figure 6. RT solid state emission spectra of complexes **1**, **2**, and **3**.

In sum, among all isomers, complex **1** shows the worst emission efficiency in both solution and solid, while complexes **2** and **3** exhibit the greatest luminescent efficiency in solid state and in degassed CH_2Cl_2 solution at RT, respectively. In solution, since all of the radiative lifetimes are nearly identical (∼10 μs), the difference in emission yield should lie in the great changes in the non-radiative decay rate constant, k_{nr}, which is in the order of **1** (3.4×10^8 s^{-1}) > **2** (9.9×10^7 s^{-1}) > **3** (1.1×10^7 s^{-1}) (see Table 3). According to frontier orbital analyses, the repulsive d-d transition does not appear up to as high as S_5 (or T_5) state (not shown here); thus its role as the major quenching pathway at RT can be eliminated.[32] Alternatively, we suspect that the seemingly weak bonding between Ir metal and hydride (cf. C−H bond), together with low frequency vibrations associated with the motions of dangling dbpH phosphine, may be responsible for the dominant non-radiative relaxation. Thus, as indicated by their bond distances (see Table 2), the much weakened Ir−H and $Ir-P_{(bdpH)}$ bond strength because of the *trans*-effect in **1** may qualitatively explain its worst emission efficiency in both solution and solid at RT. Conversely, the relatively stronger Ir−P bonding of the monodentate dbpH ligand in **3** may account for its least quenching effect and hence the highest emission intensity in solution among all titled complexes. Alternatively, the large amplitude motion in solid state associated with dangling dbpH motion has been highly restricted. This may lead to the unfrozen Ir−H stretching serving as a principal process for the non-radiative deactivation. Accordingly, the strongest Ir−H bonding and hence highest stretching frequency in **2**, as revealed by the Raman spectroscopic analysis (vide supra), should significantly suppress the non-radiative decay and

(32) Zalis, S.; Farrell, I. R.; Vlcek, A. *J. Am. Chem. Soc.* **2003**, *125*, 4580.

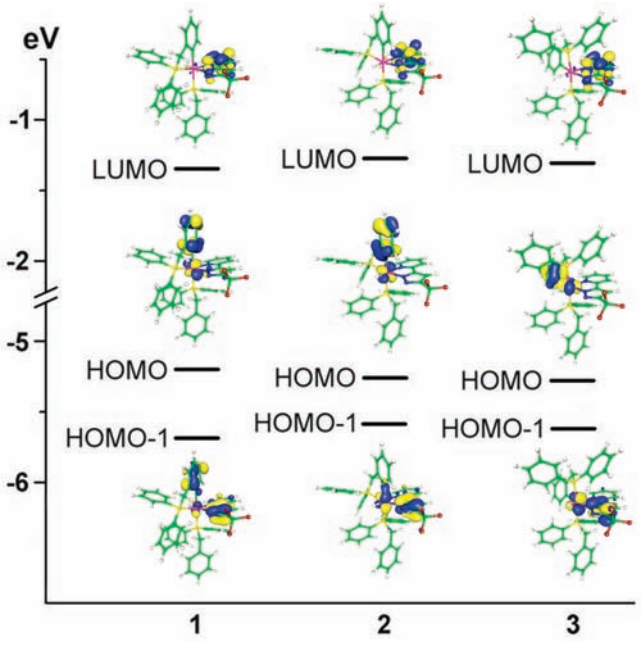

Figure 7. Selected frontier molecular orbitals mainly involved in the singlet manifold transition.

hence make this compound the best phosphor among all isomers in the solid state.

The structural and spectroscopic predictions using the DFT method were then performed to gain more insight into the titled complexes. First of all, comparisons between the calculated structures and the single crystal X-ray diffraction results were made to validate the theoretical approaches adopted in this study (see Table 2). The calculated trend of Ir−H bond strength among all complexes appears to be in qualitative agreement with the Raman spectral data (vide supra). Similarly, other structural data comparisons between the calculations and the experiments also revealed consistent results, suggesting the adequacy of the theoretical approach adopted in this study.

Next, employing the optimized ground state (S_0) structure of **1**−**3**, the TD-DFT method was then applied to investigate the gain insight into their electronic transition properties in the singlet manifold. The pertinent assignment of the frontier orbitals involved in the transition is listed in Table 4 and Figure 7. It seems that all lower lying transitions match well with respect to the experimental absorption data. For example, as for the lower lying transitions (e.g., S_1−S_3), the largest oscillator strength (*f*), that is, the S_3 state for **1** and S_2 states of **2** and **3**, are all calculated to be around ∼350 nm, which is close to the shoulder observed experimentally (see Figure 5). Moreover, the calculated $S_0 \rightarrow S_1$ transition is located at 393 nm (**1**), 374 nm (**2**), and 381 nm (**3**), and is qualitatively in agreement with the observed onsets (∼400 nm) of the absorption spectra recorded in CH_2Cl_2 solution. These results indicate that TD-DFT calculation works well in estimating the absorptive transition of the Franck−Condon excited state. Furthermore, to have a better insight into the nature of phosphorescence, the structure of the lowest triplet-state (T_1) for **1**−**3** was also optimized, and the corresponding TD-DFT calculation was then performed on the basis of these optimized structures. As a result, the transition energy and character for T_1 are listed in Table 4, while the associated frontier orbitals are depicted in Supporting Information, Figure S1. The results of molecular orbital analyses (see Table 4, Figure 7, and Supporting Information, Figure S1) indicate that both S_1 and T_1 states share a somewhat different transition pattern (Table 4). For complexes **1**−**3**, the S_1 transition is mainly involves the HOMO → LUMO transition. On the other hand, also shown in Table 4, the T_1 state is dominated by the HOMO−1 → LUMO transition for all complexes. Nevertheless, for T_1 and lower lying singlet excited state (with largest oscillator strength), the electron densities transfer is mainly from the central metal atom and the pyrazolate moiety of the fppz ligand)plus the benzyl moiety of the bdp cyclometalate in **1** predominantly) to the pyridyl fragment of the fppz chelate. The result provides further evidence for the aforementioned assignments of the lowest-energy absorption bands of **1**−**3**. Moreover, the calculated small percentages of MLCT contribution for the $T_1 \rightarrow S_0$ transitions (< 20%, see Table 4) well supports their phosphorescence originating from a dominant $\pi\pi^*$ transition, resulting in good vibronic progression and relatively long radiative lifetimes (vide supra).

Table 4. Calculated Vertical Excitation Energy and Orbital Transition Analyses for Complexes **1**−**3**[a]

cpd	states	λ_{cal}	*f*	assignments	MLCT (%)
1	T_1	514.2	0	HOMO−1→LUMO (89%) HOMO→LUMO (16%)	9.11
	S_1	393	0.0112	HOMO→LUMO (97%)	26.86
	S_2	353.9	0.0015	HOMO→LUMO+1 (83%)	23.75
	S_3	344.8	0.0161	HOMO−1→LUMO (81%)	4.87
2	T_1	522.9	0	HOMO−1→LUMO (77%) HOMO→LUMO (24%) HOMO−3→LUMO (14%)	14.52
	S_1	374.1	0.0154	HOMO→LUMO (97%)	24.00
	S_2	354.6	0.0243	HOMO−1→LUMO (85%)	19.33
	S_3	352.2	0.0014	HOMO→LUMO+1 (87%)	18.23
3	T_1	517.1	0	HOMO−1→LUMO (97%) HOMO−2→LUMO (14%)	18.08
	S_1	381.3	0.0005	HOMO→LUMO (98%)	36.44
	S_2	352.1	0.0201	HOMO−1→LUMO (87%)	29.86
	S_3	350.7	0.0018	HOMO→LUMO+1 (78%) HOMO→LUMO+2 (10%)	30.21

[a] The absorption in singlet manifold was calculated based on the optimized S_0 geometries, while triplet manifold was calculated based on the optimized T_1 geometries, respectively.

4. Conclusion

In conclusion, syntheses, spectroscopic measurements, and theoretical computations were performed on the three true-blue isomeric Ir(III) complexes **1**−**3**. In accordance to the geometry isomerism, they reveal a nearly identical emission profile but a great difference in view of luminescence intensity. This is demonstrated by the fact that complex **1** shows the worst emission efficiency, while complexes **2** and **3** exhibit the greatest luminescent efficiency in solid state and in degassed CH_2Cl_2 solution at RT, respectively. For the phosphorescence, the transition characters of these complexes are mainly attributed to the $^3\pi\pi^*$ mixed with small extent (< 20%) of ^{3}MLCT, the composition of which is further confirmed by the TD-DFT approaches. The largest k_{nr}, that is, the highest quenching efficiency, of **1** can be tentatively rationalized by the weakened dative bonding between iridium metal and

hydride as well as the monodentate benzyl diphenylphosphine. Since the true-blue phosphors are both emergent and challenging issues from the viewpoint of syntheses, this structural relationship would encourage scientists to initiate comparative research work on how to design better blue phosphors and to improve the efficiency of all phosphorescent OLEDs by controlling the coordination geometry.

Acknowledgment. This work was supported by the National Science Council and Ministry of Economic Affairs of Taiwan. We are also grateful to the National Center for High-Performance Computing for computer time and facilities.

Supporting Information Available: Figures of frontier orbitals based on the T_1 optimized geometries, and the Cartesian coordinates of fully optimized structures, X-ray crystallographic data files (CIF) of complexes **1**−**3**. This material is available free of charge via the Internet at http://pubs.acs.org.